GENERATION AND DETECTION OF VERY HIGH FREQUENCY ACOUSTIC WAVES IN SOLIDS

J. de Klerk
J. H. Parker, Jr.
R. W. Weinert
P. G. Klemens

Westinghouse Research Laboratories
Pittsburgh, Pennsylvania 15235

Contract No. NAS8-18023

Requisition No. DCN 1-7-28-00049 (I.F.)

Final Report

September 15, 1967

Prepared for

NATIONAL AERONAUTICS & SPACE ADMINISTRATION
GEORGE C. MARSHALL SPACE FLIGHT CENTER
HUNTSVILLE, ALABAMA 35812

TABLE OF CONTENTS

Abstract

The purpose of this contract is to develop techniques for generating and detecting coherent acoustic waves in solids in the frequency range above 100 GHz. During the first year of the contract advances have been made both in the areas of detection and generation. Techniques were first developed for detecting phonons in the range of 1-3 GHz by optical Bragg scattering. In this case the phonons were generated by thin film transducer techniques and interferometric methods were used for separating the frequency shifted light component. Concurrently, a Q-spoiled CO_2 laser was developed for phonon generation. This laser yielded ten infrared lines with a total peak power of 100 KW. It was estimated that at this power level the laser could initiate an acoustic wave with a strain amplitude of 10^{-6} through electrostrictive action at the surface of a crystal. The above techniques were then combined in an attempt to generate and detect phonons in α-Al_2O_3 at 54 GHz. The results of this first try have, so far, been negative. The reasons for the negative results are discussed along with the future direction of the program. A theoretical study was carried on concurrently with the above experimental work and was concerned with attenuation of high-frequency phonons in solids at low temperatures. This work has demonstrated that the acoustic attenuation will vary as the fifth power of frequency and will be quite small below 10^{12} Hz.

I. INTRODUCTION

There are many reasons that justify the development of techniques for generating and detecting coherent acoustic waves (acoustic phonons) in solids. On one hand, these techniques are important for obtaining basic information about the physical properties of crystals. For example, the basic mechanisms of many phenomenological properties of crystals, e.g., specific heat, thermal conductivity, thermal expansion and luminescent behavior of impurity ions, depend in detail on acoustic phonons and their interaction with each other and with the electronic parts of the crystal.[1] Also, these techniques are an important part of many technological devices. For example, in high frequency delay lines, in data processing devices and in defect detectors for solids.[2] There are, therefore, both scientific and technological reasons for expanding and developing techniques and methods for the generation and detection of acoustic phonons in solids.

Two of the most important methods used to generate and detect coherent acoustic waves in solids depend on the effect of an applied electric field on the elastic and dielectric behavior of the solid. These effects can be described by the following two equations,

$$\sigma = c\epsilon + dcE - \frac{k^2 pE^2}{8\pi} \tag{1}$$

$$P = XE + dc\epsilon - \frac{k^2 p\epsilon E}{4\pi} \tag{2}$$

Equation (1) relates the stress, σ, to the strain, ϵ, and to the electric field E and Eq. (2) relates the dipole moment per unit volume, P, to the same two quantities. These quantities, of course, are time and position dependent when used to describe the generation and detection of acoustic waves in solids. The first term in Eq. (1) represents the elastic behavior of solid in terms of the elastic constant, c, while the first term in Eq. (2) represents the polarizability of the solid in terms of the polarizability constant X. The second and third terms of both Eqs. (1) and (2) represent respectively, the piezoelectric and electrostrictive effects and are given in terms of the piezoelectric constants, d, and the electrostrictive or photoelastic constants, p. The constant k in these equations is the ordinary dielectric constant. It is to be noted the summation indices, which would be expected to appear in Eqs. (1) and (2) and are required because of their tensor character, have been suppressed for simplicity and physical clarity.[3] Equation (1) is the basic equation for phonon generation. It gives the stress that is induced in a crystal due to an applied electric field and if the electric field is time dependent, the induced stress can act as the driving force for initiating an acoustic wave. Equation (2) which is the basic equation for detection relates the induced dipole moment to strain. Therefore the strain due to an elastic wave can be measured electrically via the induced dipole moment. These equations indicate that both the piezoelectric and the electrostrictive effect can be used to initiate and detect an acoustic phonon.

Piezoelectric Method -- This method is the most common one used for generation and detection. At frequencies of about 100 MHz and below, the method takes the form of quartz transducers for both initiating and receiving the acoustic wave.[4] In this case the quartz transducer is bonded onto the sample. For generation, an ac electric potential is applied across the transducer which results in a wave being initiated into the sample; for detection, the ac electric potential induced across the transducer from the acoustic wave passing into the transducer is measured. In the frequency range of about 500 MHz to 100 GHz bulk quartz transducers become very inefficient. Therefore at these frequencies for piezoelectric samples, the acoustic wave is generated by surface excitation of the sample itself; for non-piezoelectric samples, thin film transducers are used.[5] The upper frequency limit to the piezoelectric techniques is about 100 GHz and this is set by the lack of coherent electromagnetic wave generators above this frequency. At a time when far-infrared lasers are developed for frequencies above 100 GHz, thin film piezoelectric techniques will probably be used in this high frequency region.

Electrostrictive Method -- The third terms of Eqs. (1) and (2) describe the basis for this method. Equation (1) implies that if two different electric fields are applied to a crystal, one with frequency ω_1 and the other with ω_2, then a stress will be produced at the difference frequency $(\omega_1 - \omega_2)$. That is, the superposition of two electric fields in a crystal will initiate an acoustic wave with a frequency given by the difference frequency of the applied fields. In turn, Eq. (2) implies that if a strain is present in a crystal, varying at a frequency of Ω, and an

electric field is applied with frequency ω, then a dipole moment will be induced in the crystal at frequencies of $\omega \pm \Omega$. It is this effect which allows an acoustic wave to be detected through the electrostrictive (or photoelastic) effect. That is, suppose an acoustic wave is present in a transparent crystal. If a light (electromagnetic) wave is sent through the crystal and across the acoustic wave, a dipole moment will be induced at all points common to the light and acoustic wave. This induced dipole moment can in turn generate an optical wave at the frequencies $\omega \pm \Omega$ and this wave, when detected will indicate the presence of the acoustic wave in the crystal. The electrostrictive effect has been used for many years for detecting and measuring the properties of acoustic waves in solids.[6] For example, the second and third order elastic constants of certain crystals have been obtained using this technique.[7] Also the first detection of coherent waves in the GHz region was carried out by this technique.[8] This method is also the basis of detecting the incoherent thermal waves in Brillouin and Raman scattering experiments.[9] There have been a few experiments which have used this method for generating coherent acoustic phonons. One of these was the first observation of stimulated Brillouin scattering in solids.[10] In this experiment a ruby laser beam is focussed into a transparent sample; this beam interacts with the thermal acoustic waves to generate a scattered light wave which in turn also interacts with the original light wave to generate new acoustic phonons. This process results in a build-up of both the acoustic phonons and the shifted frequency light beam. In another experiment[11] part of a He-Ne laser beam was shifted in frequency by

interacting with acoustic wave generated by transducer techniques at 500 MHz. This frequency shifted beam is, in turn, mixed with the original laser beam, in a crystal to generate through electrostriction, an acoustic wave at 500 MHz.

It was the purpose of the present study to develop techniques for generating and detecting acoustic waves above the 100 GHz level. The most promising method appeared to be through the electrostrictive effect. It was anticipated that the detection could be handled by using visible gas laser lines (He-Ne or argon lasers) and interferrometer or monochromator frequency resolution for observing the scattered frequency shifted optical lines. The most promising source for generation appeared to be the Q-spoiled CO_2 laser. The data that was available[12] indicated that the laser would give a whole series of lines around 10μ (1000 cm^{-1}) with approximately equal spacing of about 2 cm^{-1}. This would mean that acoustic waves could be generated at multiples of about 60 GHz, i.e., at 60 GHz, 120 GHz, 180 GHz, etc.

Therefore, the immediate objectives of this project were (1) to develop techniques and experience in detecting GHz acoustic waves by the electrostrictive effect and (2) to develop a Q-spoiled CO_2 laser that would yield the required power for generation. This report will present the progress that has been made during the first year of the present contract toward the above objectives.

Theoretical work done under this contract concerned with acoustic wave attenuation is in the form of a paper titled "Decay of High-Frequency Longitudinal Phonons" by P.G. Klemens and is included in this report as Appendix I.

II. GENERATION

Theory -- The best way to discuss the generation of acoustic waves by means of the electrostrictive effect is to return to Eq. (1) and rewrite it to include only the electrostrictive term, i.e.

$$\sigma = \frac{pk^2}{8\pi} E^2 = \frac{k^2 p}{8\pi} (E_1 + E_2)^2 \qquad (3)$$

where E_1 and E_2 represents the electric fields of two distinct electromagnetic waves. These fields would be given individually by

$$E_1 = e_1 \sin(\omega_1 t - \underline{K}_1 \cdot r)$$

and

$$E_2 = e_2 \sin(\omega_2 t - \underline{K}_2 \cdot r) \ ,$$

where ω_1 and ω_2 are the frequencies and $\underline{K}_1$ and $\underline{K}_2$ are the wave vectors of the respective waves. It is assumed for simplicity that E_1 and E_2 are parallel. Then the component of σ that oscillates at the difference frequency, $(\omega_1 - \omega_2)$, is given by

$$\sigma = \frac{k^2 p e_1 e_2}{8\pi} \cos\left[(\omega_1 - \omega_2)t + (\underline{K}_1 - \underline{K}_2)\cdot r\right] \qquad (4)$$

The stress given by Eq. (4) now becomes the driving term for an elastic wave equation, i.e.,

$$\frac{1}{V^2}\frac{\partial^2 U}{\partial t^2} - \frac{\partial^2 U}{\partial x^2} = \frac{1}{c}\frac{\partial \sigma}{\partial x} \quad ,$$

where U is the local particle displacement, V the acoustic phase velocity in the crystal and x the distance along the acoustic wave normal. It must again be pointed out that the present discussion is somewhat qualitative in that the tensor character of the quantities involved has been ignored and that the above wave equation is somewhat simplified. Under certain conditions the driving stress wave given by Eq. (4) can be matched in phase velocity to an acoustic wave in the crystal. The conditions for this are,

$$\omega_1 - \omega_2 = \Omega$$

and

$$\underline{K}_1 - \underline{K}_2 = q,$$

where Ω is the frequency and q the wave vector of an acoustic mode in the crystal. This means that if the crystal can support an acoustic wave with the above frequency and wave vector, then the stress wave (Eq. 4) over its entire volume of action will act as a spatially coherent source for this acoustic wave. It is clear that this case of spatially coherent generation can only occur when the acoustic wavelength is smaller or of the order of the optical wavelength in the crystal. The two studies[10,11] which were referred to in the Introduction of this report, in which the electrostrictive effect is employed for generation, depended on this

type of spatial coherence. In the present case where infrared optical waves are to be used for generation, these conditions cannot be met because the optical wavelength is large in comparison to the acoustic wavelength. Even though these conditions cannot be satisfied, the stress given by Eq. (4) can still act as a driving source for generation at the surface of the crystal. This means that if two optical waves are sent into a crystal at a common point on its surface, these waves will interact at the surface, because of the discontinuity in the photoelastic constant, to yield a driving force at the surface that will initiate the acoustic wave. The stress wave given by Eq. (4) will still exist inside the crystal but its net effect will be zero. The wave equation with surface excitation is given by

$$\frac{1}{V^2}\frac{\partial^2 U}{\partial t^2} - \frac{\partial^2 U}{\partial x^2} = \frac{\delta(x) k^2 p e_1 e_2}{8\pi c} \cos(\omega_1 - \omega_2)t \quad ,$$

where $\delta(x)$ is the Dirac delta function and it is assumed that the two light waves are incident on the $x = 0$ plane. The strain amplitude of the acoustic wave that is initiated at the surface is then given by

$$\epsilon = \frac{k^2 p e_1 e_2}{8\pi c} \quad .$$

This can be written as

$$\epsilon = \frac{k^2 p F}{2c\, c_\ell\, A} \times 10^7 \quad ,$$

where F is the laser power (watts) in each of the two lines that are being mixed, A is the area (cm^2) of the laser beam on the crystal surface, and c_ℓ is the velocity (cm/sec) of light. If we assume that the laser power is 10 Kw, that the laser beam is focused to a spot size of 10^{-5} cm^2 (0.03 mm square), and we take the elastic constant, c, to be equal to 5×10^{11} dynes/cm^2, the photoelastic constant, p, to be 0.3 and the dielectric constant, k, to be 3, then the strain is

$$\epsilon \simeq 10^{-6} .$$

This corresponds to an acoustical power density of about 10 mw/cm^2. It is evident, therefore, that if the laser power is of the order of 10 Kw for the individual CO_2 lines, then a finite strain wave can be initiated at the surface of a crystal.

CO_2 Laser Tube -- The theory of the laser and, in particular, the theory of the CO_2 laser will only be discussed qualitatively since both subjects are adequately covered in the literature.[13,14] The laser is an optical oscillator capable of yielding coherent optical power. The two essential parts of a laser are (1) a medium that has power gain at optical frequencies and (2) a means for feedback at these optical frequencies. The amplifying medium can consist of ions, atoms or molecules, either in a gas or solid phase, which have, as a whole, a non-equilibrium, population inversion of their energy levels. This inverted population can lead to power gain for an electromagnetic wave through stimulated emission. Optical mirrors act as the feedback which turns the amplifying medium into an oscillator.

It is the CO_2 molecule which has some of its vibrational energy levels inverted that gives the required optical gain for the CO_2 laser. In this case an electrical discharge acts as the inverting pump. Nitrogen and helium are added to the discharge to enhance the inversion of the CO_2 levels.

A laser can be operated either as steady state oscillator or as a pulsed oscillator. The Q-spoiled laser is a type of pulsed laser where the feedback is suddenly turned on with the result that the oscillations build up to a very high level. One common method for feedback turn on makes use of a rotating mirror. This is the method that has been used for Q-spoiled CO_2 lasers.[15]

The important objective of this part of the program was to construct a Q-spoiled CO_2 laser that would deliver Q-spoiled pulses made up of individual CO_2 laser lines each with peak powers as large as possible. While available data from other investigators[15] indicated that total peak powers of the order of at least 50 Kw could be realized, there was no data at the start of this program on the distribution of this energy among the various CO_2 laser lines.

The first laser tube that was constructed was made up of 4" I.D. pyrex pipe with concentric water jackets of fiberglass tubing bonded to the pyrex with epoxy resin. The length of the active discharge was 8 ft. and used 3" diam. mirrors internal to the discharge tube. This tube was operated only in a continuous mode and delivered the order of 100 watts.

It was decided that a smaller diameter tube would be more suitable for Q-spoiled operation. This tube in its final form is shown

schematically in Fig. 1. Figure 2 shows a photograph of the tube. The tube is constructed of pyrex pipe, but now with a 2" I.D. The water jackets are formed by using commercial fiberglass tubing bonded and sealed to the outside of the pyrex pipe with epoxy resin. This tube is made up of four sections of 4 ft long pipe with three electrodes, one on each end and one in the middle. This yields an active discharge length of 16 ft. (5 meters). At each end, the pyrex pipe is expanded into a larger diameter so as to accommodate the mirror mounts. The tube is pumped at one end and the gas is fed in at the other. Initially the tube was pumped with one 15 ft^3/min pump. This pumping rate was not fast enough to prevent decomposition of the CO_2 and N_2 as was evident from the variation in discharge color along the length of the tube. The smaller pump was replaced by 50 ft^3/min pump which resulted in a much more uniform discharge and in a somewhat higher output. The mirror mounts at one end were constructed so that either a fixed mirror or rotating mirror could be mounted. The mirror at the other end was fixed and was concave with a radius of curvature equal to the length of the tube. This gave a hemispherical laser cavity configuration when the rotating mirror was plane. This configuration was convenient in that only a small (1/2" x 1/2") rotating mirror was required. The mirrors were fabricated of quartz with gold reflecting coatings. The output was obtained by aperture coupling through the center of the permanent mirror and the output was passed out of the tube through an Irtran IV window. The three gases, CO_2, N_2 and He, were fed from high pressure (Airco) tanks through variable (Granville-Phillips)

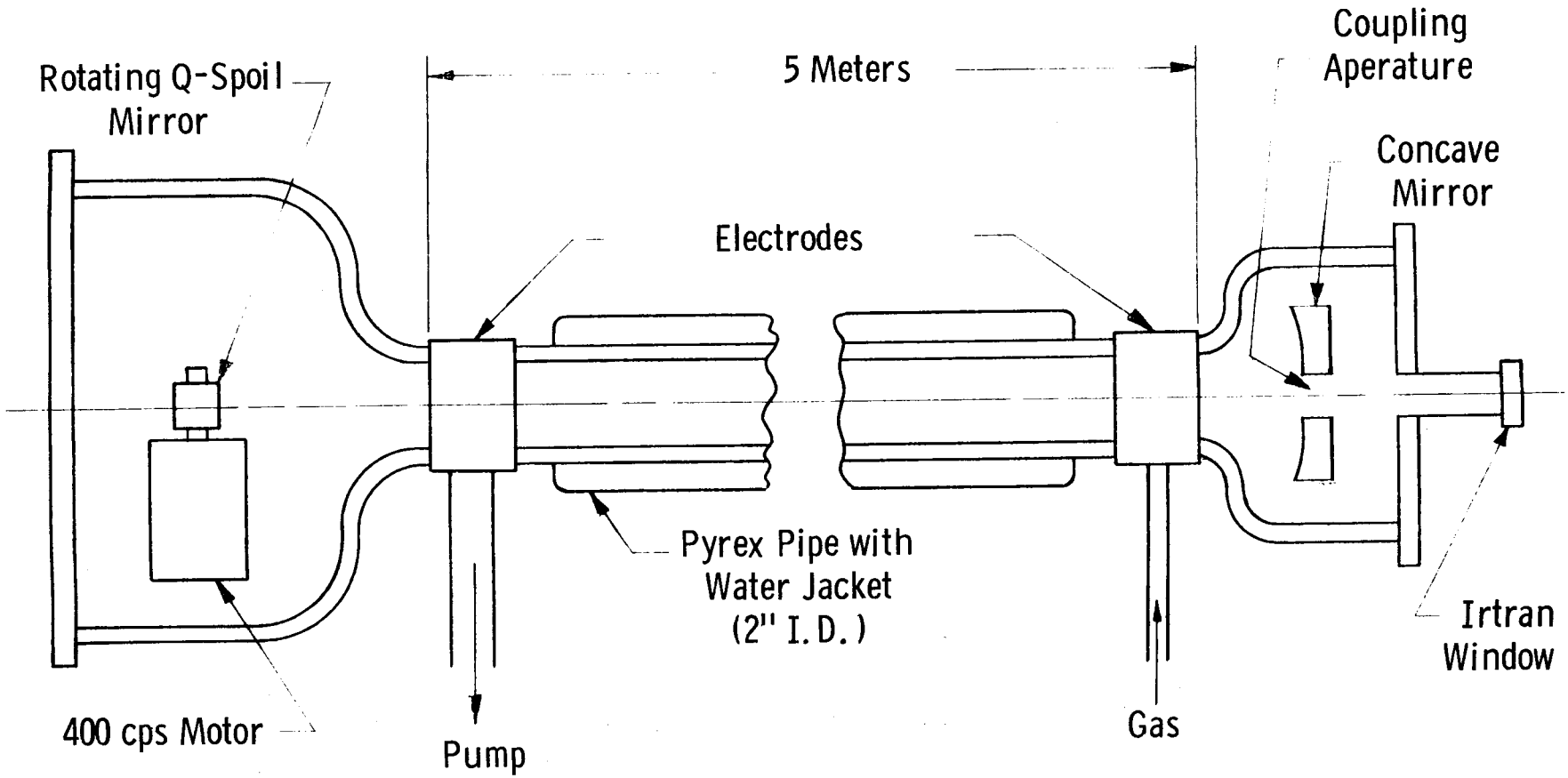

Schematic diagram of CO_2 laser

Fig. 1

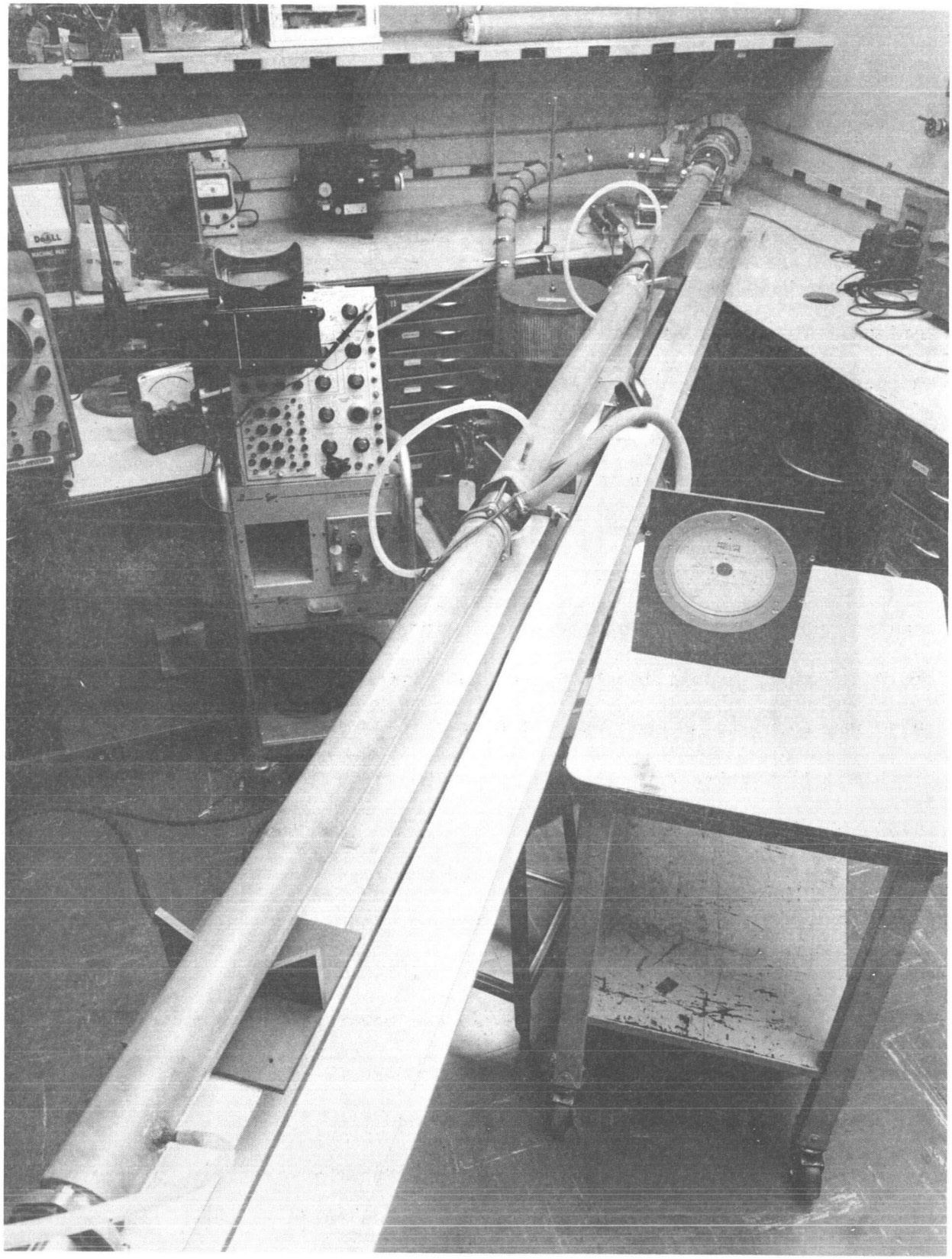

Q-Spoiled Laser Tube

Fig. 2

leaks into the tube. The pressure in the tube was measured by a Wallace and Tierman precision pressure dial gauge. The DC power for the discharge was obtained from a full wave rectified three phase supply. The supply could deliver up to 15 KV at 100 ma and was controlled by three ganged Variacs. The discharge was operated as two parallel sections; that is, the center electrode acted as a common cathode for the two anode electrodes at the ends of the tube. The ballast resistance in each discharge leg was 40 KΩ. Table I gives the important characteristics of the discharge. This tube gave the order of 200 watts in CW operation.

In the first try at Q-spoiled operation, a 60 cps motor was used for rotating a square, four-faced mirror. This arrangement gave a 240 sec^{-1} pulse repetition rate. At this speed of rotation, the total pulse was found to be made up of two or three smaller pulses, each with risetimes of the order of 1-2 μs. This indicated that the 60 cps rotary speed was too slow. A 400 cps motor was installed and as a result almost all the multiple pulses disappeared, and the rise time was decreased to the order of 0.1 μs. Table II gives some of the laser characteristics when operated at the 400 sec^{-1} pulse repetition rate. The energy per pulse was obtained by measuring the average power with a Westinghouse laser calometer and dividing this number by the known pulse repetition rate. The peak power in a simple pulse was obtained from the energy per pulse and from the pulse width as measured by a Ge-Au photoconductive cell. Figure 3 gives a drawing of a typical Q-spoiled pulse as taken from an oscilloscope photograph.

Table I

DISCHARGE CHARACTERISTICS

Discharge current	70 ma
He pressure	4 Torr
N_2 pressure	1 Torr
CO_2 pressure	0.5 Torr
Pumping speed	50 ft^3/min
Discharge length	16 ft
Discharge diameter	2 in

Table II

Q-SPOILED LASER CHARACTERISTICS

Cavity configuration	Hemispherical
Energy per pulse	20 mjoule
Pulse rate	400 sec^{-1}
Pulse width	0.2 μs
Total peak power	100 KW
Number of strong lines	10

It is to be noted that while the rise time of the pulse as given in Fig. 3 is close to the true rise time, the fall time is limited by the time constant of the measuring circuit and is therefore somewhat longer than the true fall time. The resolved spectra of laser output is shown in Fig. 4. This was obtained with a NaCl prism monochromator in conjunction with a radiation thermopile. It is seen that the spectra is made up of two groups of lines. The first group has a spacing of 2 cm^{-1} and the second group has a spacing of 1.8 cm^{-1}. It is to be noted that while the first group is reasonably well resolved, the second group just gives a hint of its line structure. This is due to the finite resolution of the monochromator that was used for this measurement. It can be seen that there are about 10 strong lines. It is the group with lines spaced at 1.8 cm^{-1} or 54 GHz that were used, as described in the next section, for a first try at generation and detection of 54 GHz phonons.

Future Plans -- There are many aspects of the Q-spoiled laser that need further work and development. The most essential is to increase the peak power, either by decreasing the pulse width or increasing the energy per pulse. The energy per pulse can, in principle, be increased by making the laser tube longer. However, this may also increase the pulse width. The dependence of these quantities, i.e., pulse width and energy, on such parameters as the rotation speed of the Q-spoil mirror, the length of the laser and the amount of output coupling need further investigation. Another avenue that should be investigated is the use of a laser oscillator plus an amplifier to obtain the required peak power. Also, more detailed work is needed on the resolved spectra of the Q-spoiled laser and how the length of the laser tube affects this spectra.

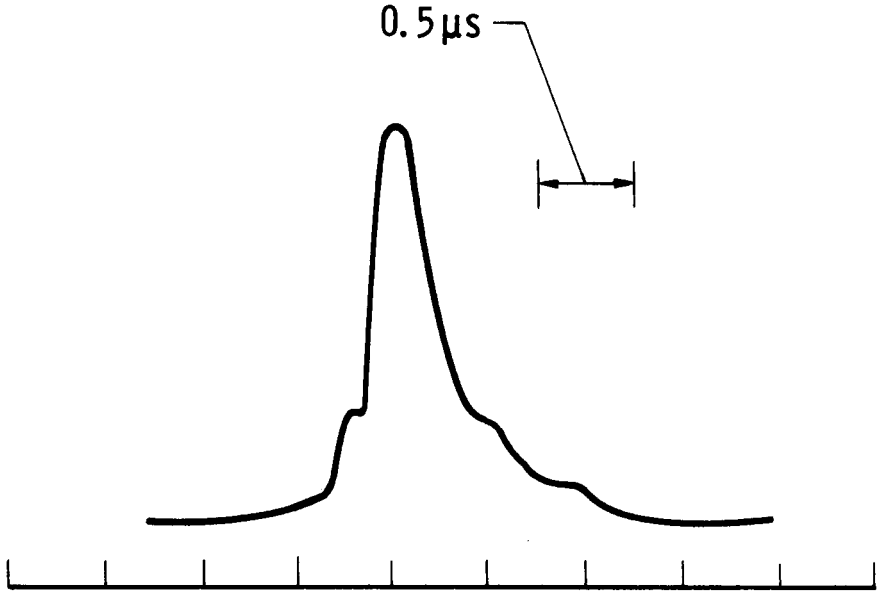

Q-Spoiled Pulse

Fig. 3

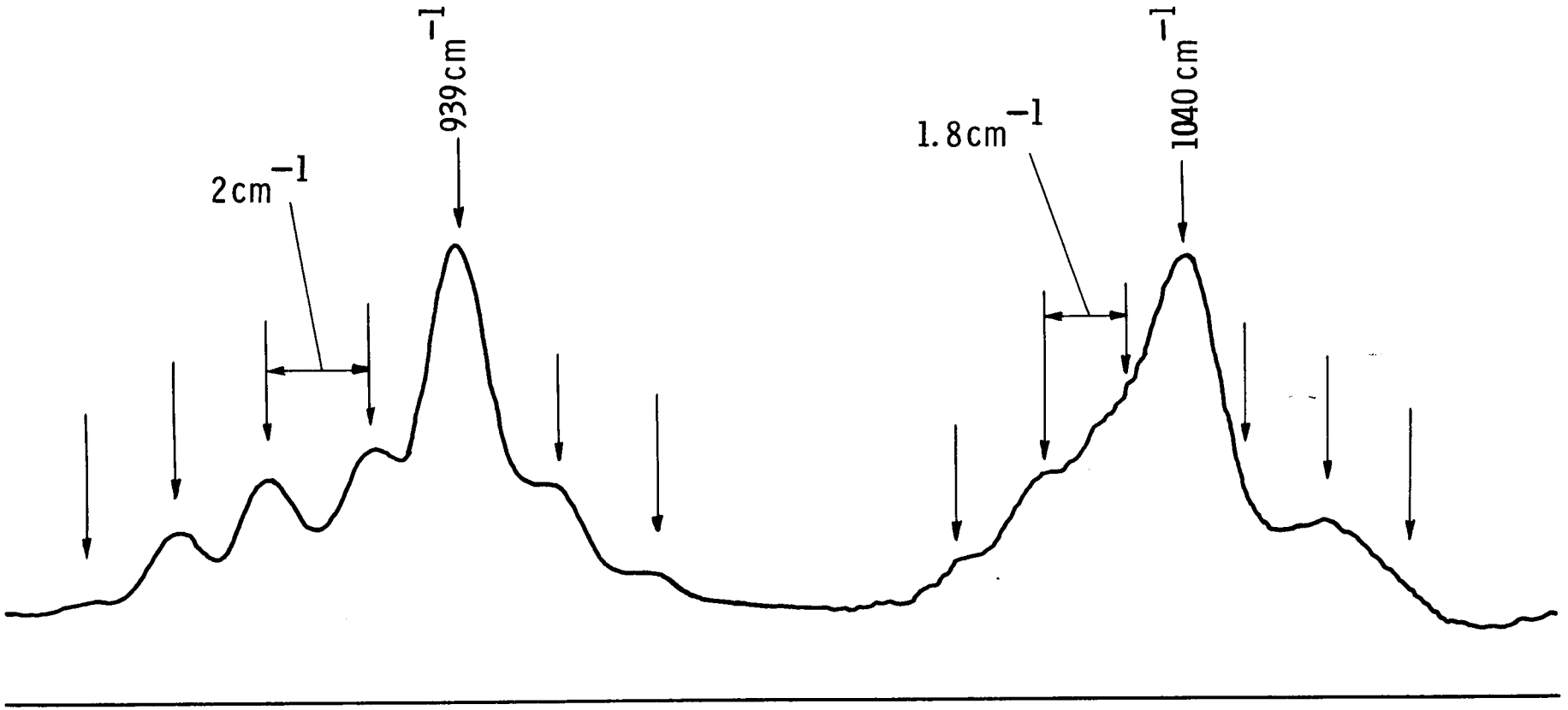

Infrared Spectra From Q-Spoiled Laser

Fig. 4

III. DETECTION

Simple Theory

The diffraction of light by acoustic waves in transparent solids and liquids is not a new technique as was mentioned in Section I. Since the advent of the laser and improved experimental techniques for generating acoustic waves in the microwave range, there has been renewed interest in this interaction. The diffraction of light by coherent acoustic beams in solids is especially strong for a particular angle of incidence and scattering angle of the light beam relative to the sound wave propagation vector $\underline{q}$. The particular angle of incidence θ_1 is called the Bragg angle for the scattering of light by acoustic waves. Since the theory of Bragg angle scattering has been well covered in the literature recently,[16,17] only a brief sketch of the theory will be presented here.

The model for the discussion is shown in Fig. 5. The longitudinal acoustic wave propagation vector and frequency are $\underline{q}$ and Ω respectively, and the incident light is denoted by its propagation vector $\underline{K}_i$ and frequency ω_i. Two rays of the light beam, rays 1 and 2, are shown and are incident at an angle θ_i relative to the $\underline{q}$ vector normal. Since for most materials the velocity of the acoustic wave (10^5 to 10^6 cm/sec) is much less than the velocity of light in the medium (10^9 to 10^{10} cm/sec), the acoustic wave fronts can be thought of as stationary during the time the light rays pass through the acoustic disturbance. The shaded and unshaded areas in Fig. 5A very schematically represent the different

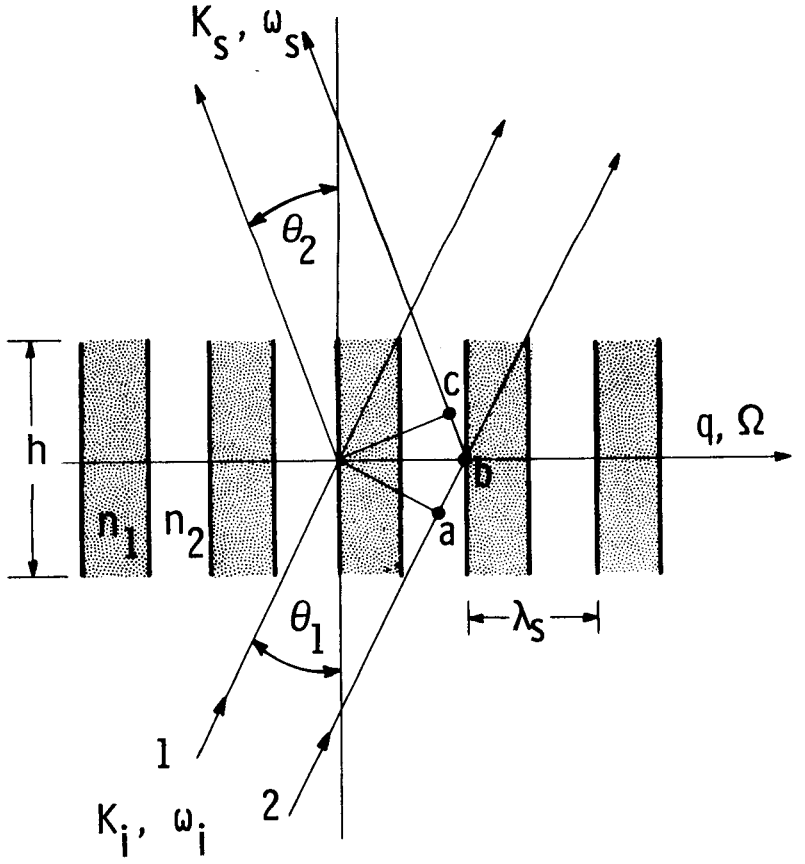

$$\theta_1 \approx \theta_2 = \theta_B$$
$$n_1 = n + \Delta n$$
$$n_2 = n - \Delta n$$

(A)

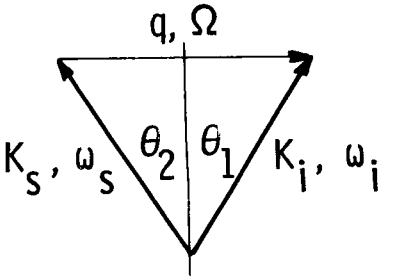

$$\omega_i = \omega_s + \Omega$$
$$\vec{K}_i = \vec{K}_s + \vec{q}$$
$$K_i \cos\theta_1 = K_s \cos\theta_2$$
$$K_i \sin\theta_1 + K_s \sin\theta_2 = q$$

(B)

Fig. 5—Schematic representation of interaction of light waves and acoustic waves

index of refraction regions caused by the strain produced by the acoustic wave. For the case where the acoustic wave fronts are thought of as being stationary, $\theta_1 = \theta_2$. And, for particular values of $\underline{K}_i$ and $\underline{q}$ there is an angle of incidence $\theta_1 = \theta_B$ such that ray 1 and ray 2 differ in phase by 2π upon emerging from the acoustically disturbed region. That is when the wavelength of sound λ_s, the wavelength of light in the medium λ_i, and the incident angle θ_B satisfy the equation

$$\sin \theta_B = \frac{\lambda_i}{2\lambda_s} , \tag{5}$$

then the scattered light due to rays 1 and 2 interfere constructively. This can be seen easily by showing that the optical path difference (ab + bc) between rays 1 and 2 is equal to the wavelength of light in the medium when $\theta_1 = \theta_B$. The situation can be stated by saying that momentum is conserved during the scattering process. This is shown in part B of Fig. 5. That energy is also conserved during the interaction implies that the scattered light frequency must differ from the incident light frequency by the acoustic frequency. The frequency shift, however, is a consequence of the acoustic velocity V_s. (The frequency shift can be thought of for the simple model of Fig. 5A as arising from a Doppler shift due to the finite velocity of the acoustic waves.) Therefore, in the strictest sense Eq. (5), which ignores V_s, is only an approximation as was mentioned above. But the approximation inherent in Eq. (5) is a good one when it is desired to calculate the Bragg angle from the simple

model of Fig. 5A. The above ideas considered with Fig. 5 are simple and show that there is a particular angle of incidence of light relative to the acoustic column which leads to a reinforced, frequency shifted, scattered beam of light.

Acoustic Frequency Range Considerations

According to Eq. (5) reinforced scattering can occur as long as $\frac{\lambda_i}{2\lambda_s}$ is less than or equal to one. For values of $\frac{\lambda_i}{2\lambda_s} > 1$, reinforced scattering from many acoustic waves cannot take place. The upper limit acoustic frequency Ω_B depends on the velocity of the acoustic waves and the wavelength of light used to detect them. For longitudinal waves in x-cut quartz ($V_s = 5.72 \times 10^5$ cm/sec),[8] $\Omega_B = 27.8$ GHz, and for longitudinal waves in a-cut sapphire ($V_s = 11.03 \times 10^5$ cm/sec),[18] $\Omega_B = 61.5$ GHz. Both of these values are stated for $\lambda_i = 6328$ Å in air. It is true that for most materials Ω_B is much less than 10^{11} Hz. Since it is desired to use the light-sound interaction to eventually detect acoustic waves with frequencies up to 10^{12} Hz, methods of detection must be discussed which do not involve Bragg scattering. To appreciate the differences between Bragg scattering at frequencies much less than Ω_B and frequencies near Ω_B, either under or over, both regions will be considered separately.

Experiment $\Omega < \Omega_B$

Equipment -- The experimental arrangement for Bragg angle scattering is shown in Fig. 6. The laser used in all of this work was a modified Perkin & Elmer He-Ne laser. The modifications consisted of a 1/2" thick invar plate, which served as a base, and new mirror mounts specially designed for rigidity and ease of alignment. The laser cavity was slightly less than 1 meter in length and power outputs were between 1 and 10 mw depending on the age of the plasma tube and the mode pattern[19] in which the laser was operating. The optical isolator shown in Fig. 6 consists of a 1/4 wave plate and polarizer and prevents any back-scattered light from interfering with the operating of the laser. The sample holder was mounted on a rotating table which allowed absolute settings to within 0.1° and rotations fine enough to mechanically scan angular regions of 0.05° extent. Provisions were made to observe the "straight through" undiffracted laser beam and the Bragg diffracted beam. This was done, as indicated in Fig. 6, with a mirror and beam splitter. Either one of these beams, or both, were sent into a photomultiplier, and the multiplier output was fed into a scope when the acoustic waves were in the form of pulses, or into a DC μ-ammeter, when the acoustic waves were c.w. A Fabry-Perot interferrometer[19] was sometimes placed between the sample and the photomultiplier for reasons which will be discussed later when the frequency range $\Omega \sim \Omega_B$ is considered. The set-up shown in Fig. 6 was used for acoustic frequencies between 0.9 and 3.0 GHz.

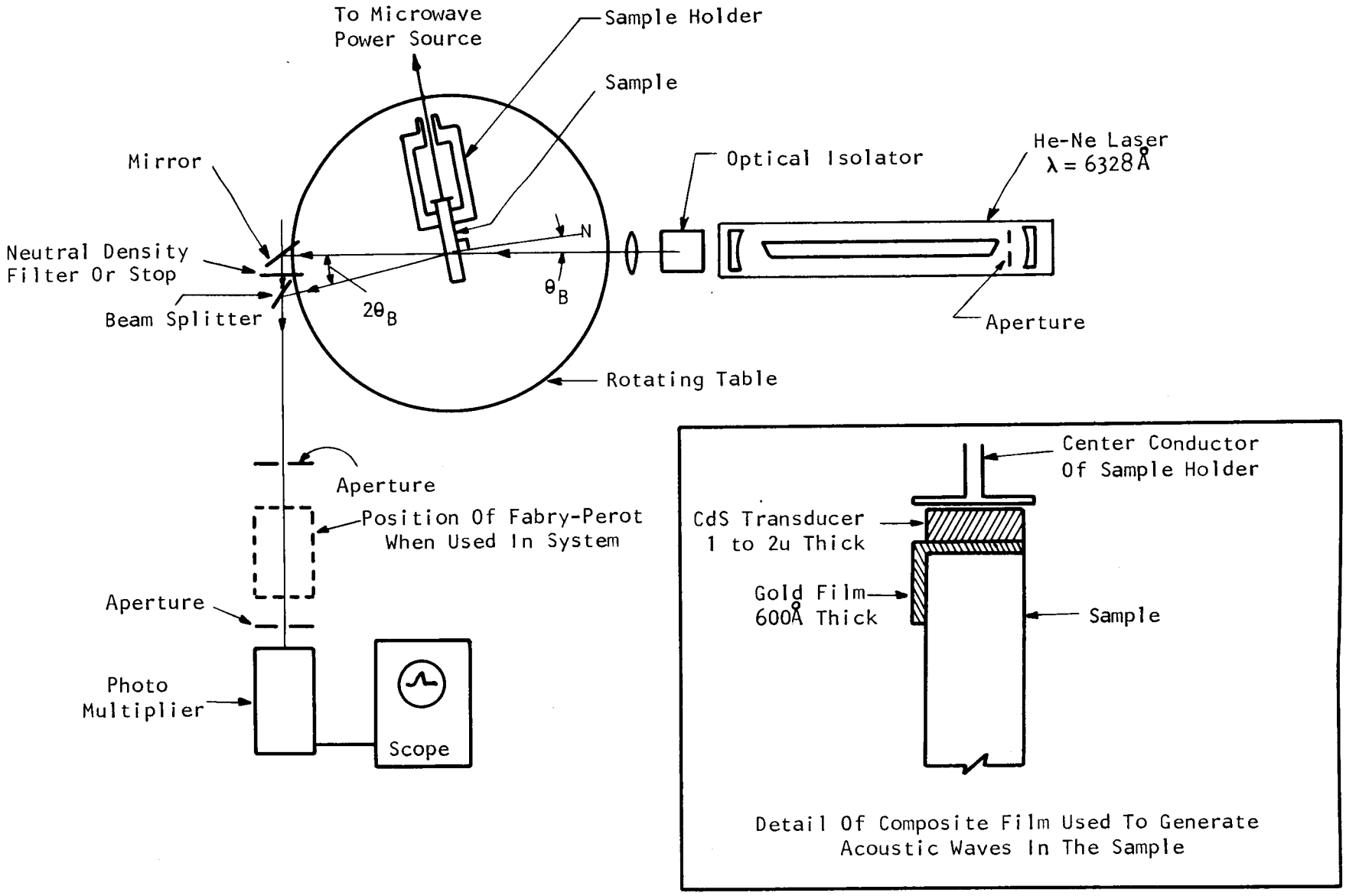

Fig. 6—Experimental arrangement for Bragg scattering for acoustic frequencies in the range of 1 to 3 GHz

Sample Considerations -- The samples used in the low frequency Bragg scattering experiments were 1/4" square cross-sectional pieces of quartz and sapphire. The sample lengths varied from 0.3 cm to almost 4 cm. The end faces were parallel to 10 seconds of arc and flat to 1/10 wave. The long side faces were parallel to 15 seconds of arc, perpendicular to the end faces to within 15 minutes of arc, and flat to 1/10 waves. Most of the samples used in this work were supplied by the Valpey Corp.

It is very important that the long side faces be optically flat and clean. As can be seen from Fig. 6, the diffracted beam of light is separated in angle ($\sim 2\theta_B$) from the main laser beam. How well the two beams are actually separated depends in part on the quality of the surfaces through which the laser beam passes. If these surfaces are not of high optical quality, part of the laser beam will be scattered into the direction where Bragg scattering is being observed and seriously affect the overall signal-to-noise ratio. Not only were the samples given a good optical finish initially, but they were also cleaned repeatedly during measurements.

Acoustic Power and Diffracted Light Powers -- The fraction of light diffracted by the acoustic waves is directly proportional to the acoustic power. Therefore, some time was spent in trying to increase the acoustic powers in the samples. Initial work with quartz samples at 1 GHz was done with high Q-microwave cavities. Because quartz is piezoelectric, acoustic waves were generated directly under the action of the microwave electric field present in the cavity. The microwave transmitter (not shown in Fig. 6) was a planar triode cavity oscillator which put out 1 kw

peak power in 1 μ-sec pulses. Repetition rates were usually set between 400 and 1000 Hz. The fraction of light diffracted by x-cut and z-cut quartz samples during the acoustic pulse using the above technique, was of the order of 10^{-5} and corresponded to peak acoustic powers of about 1 mw/cm^2. (This does not imply that the rf to acoustic power efficiency is 10^{-6} for the sample filling factor was only of the order of 10^{-3}.) In order to appreciate the fact that a measurement of the fraction of light diffracted can give a direct measurement of acoustic power in some samples, the relationship between the diffracted light intensity I_D, the incident laser intensity I_0, and the sample parameters must be discussed. It can be shown[16] that

$$\frac{I_D}{I_0} = K_i^2 \frac{n^4}{2} p_{ij}^2 \left(\frac{P_{ac}}{2V_s c_{jj}} \right) h^2 \left(\frac{\tan \theta_B}{\sin \theta_B} \right)^2 \qquad (6)$$

where K_i is the propagation vector of incident light in the medium in cm^{-1}, n is the index of refraction, and P_{ac} is the acoustic power in erg/sec-cm^2. p_{ij} and c_{jj} are the appropriate photoelastic and elastic constants respectively. In Fig. 5, if the direction of $\underline{q}$ is taken as the x-axis then the appropriate elastic constant is c_{11}, and since the light in the sample was always polarized perpendicular to the x-axis, the appropriate photoelastic coefficients for most of our work are p_{21} and p_{31}. Using Eq. (6) and the relationship between acoustic power and strain

$$P_{ac} = \frac{1}{2} V_s c_{11} \epsilon_1^2 \quad , \tag{7}$$

the relationship between I_D/I_0 and strain can be obtained. For x-cut quartz containing longitudinal waves traveling along the x-axis, 1 mw/cm^2 of acoustic power corresponds to a strain of 2.1×10^{-7}.

Some Results -- In order to increase the ratio I_D/I_0, thin film CdS transducers[20] were deposited on one end of the samples and it was found by measurement that acoustic powers greater than 10 mw/cm^2 were obtained. Finally, a composite film composed of a gold back-up electrode and a CdS transducer was used on the end of an x-cut quartz sample. This composite film is shown in detail in Fig. 6. I_D/I_0 values of 2×10^{-2} were obtained during the acoustic pulse. This ratio corresponds to peak acoustic powers of roughly 2 watts/cm^2 and peak strains equal to 1×10^{-5}. Acoustic powers of this order were obtained with composite films in a few x-cut quartz samples and a z-cut quartz sample. Using Bragg scattering in a-cut sapphire with a composite film yielded peak acoustic powers somewhat less than in quartz (0.01 to 0.1 watts/cm^2). An oscilloscope trace of the Bragg effect in a 9 mm long x-cut quartz sample at sound frequencies of 1 GHz is shown in part (a) of Fig. 7. The sample had a composite film (gold + CdS) on one end, and the light entered the sample 3.3 mm from the transducer. The upper trace is the output of a photomultiplier set at the correct scattering angle to see Bragg scattering. The second signal of the upper trace corresponds to the acoustic pulse that has been reflected from the free end of the sample (i.e., the end

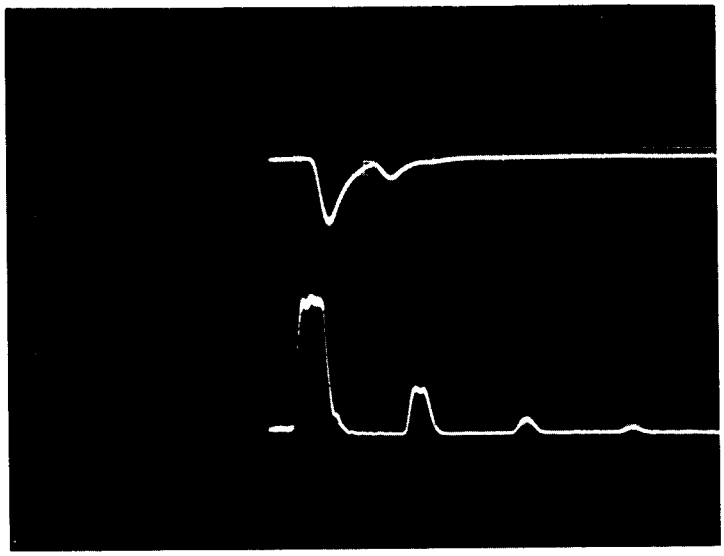

5 v/cm, $\frac{2\,\mu\text{-sec}}{\text{cm}}$

Fig. 7a—Upper Trace. Bragg effect for longitudinal waves in x-cut quartz, $\Omega = 1$ GHz
Lower Trace. Conventional pulse-echo pattern

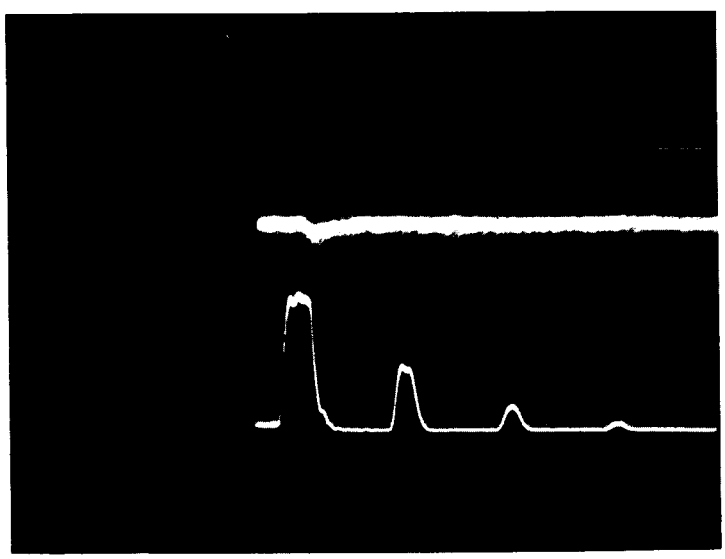

50 mv/cm, $\frac{2\,\mu\text{-sec}}{\text{cm}}$

Fig. 7b—Upper Trace. Bragg effect for 2nd harmonic wave in x-cut quartz
Lower Trace. Pulse-echo pattern, $\Omega = 1$ GHz

away from the transducer). The measured I_D/I_0 for this sample was 0.02. The lower trace in Fig. 7a is the pulse echo pattern using conventional microwave equipment. The first pulse is the transmitter pulse while the rest of the pulses are echoes. It should be pointed out that if the gain was turned up in the first trace of part (a) all of the echoes are visible via the scattered light. Part (b) of Fig. 7 shows the Bragg effect for the second harmonic acoustic wave generated in the sample of part (a). Between part (a) and part (b) only θ_B was changed from $\sim 3^\circ$ to 6°. Since the amplitude of the second harmonic signal can lead to information concerning the third order elastic constants, more work will be done in this area shortly. Photos are not shown for acoustic frequencies higher than 1 GHz but the Bragg effect was seen in x-cut quartz for acoustic frequencies up to 3 GHz.

High Frequency Considerations

The most important feature of low frequency Bragg scattering, when considering signal-to-noise, is that the frequency-shifted, scattered light beam is spatially separated from the main laser beam as is indicated in Figs. 5 and 6. Bragg scattering for frequencies below Ω_B but close to it presents certain problems caused by the high attenuation coefficient α which most substances exhibit at room temperature and high acoustic frequencies. To appreciate some of the difficulty, an a-cut sapphire rod containing 54 GHz longitudinal acoustic waves will be considered. The measured attenuation coefficient for longitudinal waves in a-cut sapphire

is 0.2 db/cm at room temperature and 1 GHz.[20] Since α goes up like the frequency squared, its value becomes 600 db/cm at frequencies of 54 GHz. This means that most of the acoustic power is contained in a region of 0.1 mm away from the surface where it is generated. This fact, coupled with the fact that the Bragg angle in the medium for 54 GHz longitudinal waves is about 61°, leads to the following complication. For normal laser spot sizes, it is impossible to sense the region containing the acoustic waves and not hit the excitation surface itself with the light beam. The specularly reflected light comes off at the same angle as the Bragg scattered light. Therefore the Bragg diffracted light must be detected in the presence of a significant fraction of the laser beam. That is, there is no spatial separation between the diffracted and undiffracted light beam. A problem which must be solved experimentally then is the separation of the small intensity, frequency shifted light from the large intensity unshifted light. Since the shift in frequency is equal to the acoustic frequency, an instrument such as a Fabry-Perot interferrometer or a high resolution monochromator must be used. A Fabry-Perot interferrometer was used in this work.

Fabry-Perot Interferrometer -- The Fabry-Perot was mounted on a 1" thick invar base. The separation between mirrors could be changed mechanically with a differential screw drive or it could be changed by applying a voltage to a piezoelectric drive mirror mount. Initially, the mirror separation was set to 10 cm. One mirror was a 98% reflecting, 1.1 m radius, spherical mirror, and the second mirror was a 95% reflecting

flat. Figure 8 shows the axial modes of the He-Ne laser. Off-axis modes were suppressed by using a small aperture within the laser cavity and in front of the Fabry-Perot. Figure 8 was obtained by sweeping the Fabry-Perot mirror separation by applying a 60 Hz sine wave to the piezoelectric drive element. The signal shown is that from a photomultiplier viewing the output of the Fabry-Perot (F.P.).

Side Experiment -- To become accustomed to using the F.P. to separate a beam of light according to its frequency, the following simple experiment was done with 1 GHz acoustic waves in x-cut quartz. A mirror was placed in the main laser beam after it had passed through the sample containing a few mw/cm^2 of cw acoustic power. The mirror was adjusted such that the main beam was sent down the same path as the Bragg diffracted beam, and is shown in Fig. 6. The beam splitter reflected part of the diffracted beam into the photomultiplier and allowed a large fraction of the laser beam to pass through it after reflecting from the mirror. Then the F.P. was placed between the beam splitter and the photomultiplier, and the mirror separation of the F.P. was swept electronically while the output of the photomultiplier was put into an oscilloscope. By placing neutral density filters in the laser beam after it had traversed the sample, it was found that the shifted component could be seen in the presence of the unshifted light when the intensity of the unshifted component was not more than 100 times greater than the frequency shifted component. That is, the F.P. used as a narrow band light filter, centered at the Bragg shifted frequency can attenuate the unshifted light by 20 db.

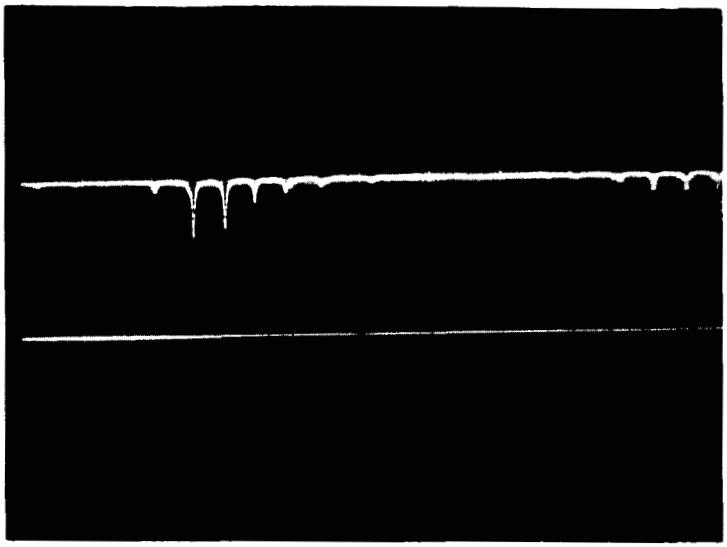

Fig. 8—Fabry-Perot scan of axial laser modes of the He-Ne laser operating at $\lambda = 6328$ Å. The Fabry-Perot spacing was 10 cm

Therefore, when the small intensity frequency shifted light and the large intensity unshifted light are not spatially separated as they will be in the final experiment to be described, the F.P. can be used to attenuate the intensity of the unshifted beam by a factor of 100.

Final Experiment -- After the preliminary results described above, an attempt to detect 54 GHz sound waves in sapphire was carried out. The experimental arrangement is shown in Fig. 9. The CO_2 laser described in Section II was used to generate the acoustic waves. Since the CO_2 laser is pulsed at 400 Hz, it was felt that there would be a definite signal-to-noise advantage by synchronously detecting the output of the F.P. The F.P. mirror spacing was 1.55 cm which corresponds to a spectral range[21] of ~9.7 GHz. Figure 10 shows the unresolved laser modes when using the F.P. at this mirror spacing. Each signal of the upper trace is composed of many laser modes. Since the scanning voltage changed the mirror separation of the F.P. by at least two spectral ranges, two such signals occur. The 3rd signal, farthest to the right, corresponds to a mirror separation identical to that yielding the 2nd signal. The sinusoidal voltage used to change the mirror separation is shown in the lower trace.

The frequency shift of the Bragg diffracted light is 54 GHz. Dividing this frequency by the spectral range of the F.P. and disregarding integer values of the spectral range yields the result that the Bragg shifted component should occupy a position the same as would light shifted in frequency by 5.8 GHz away from the laser center frequency. Figure 11a shows the output of the F.P. as it is scanned over 1 spectral range,

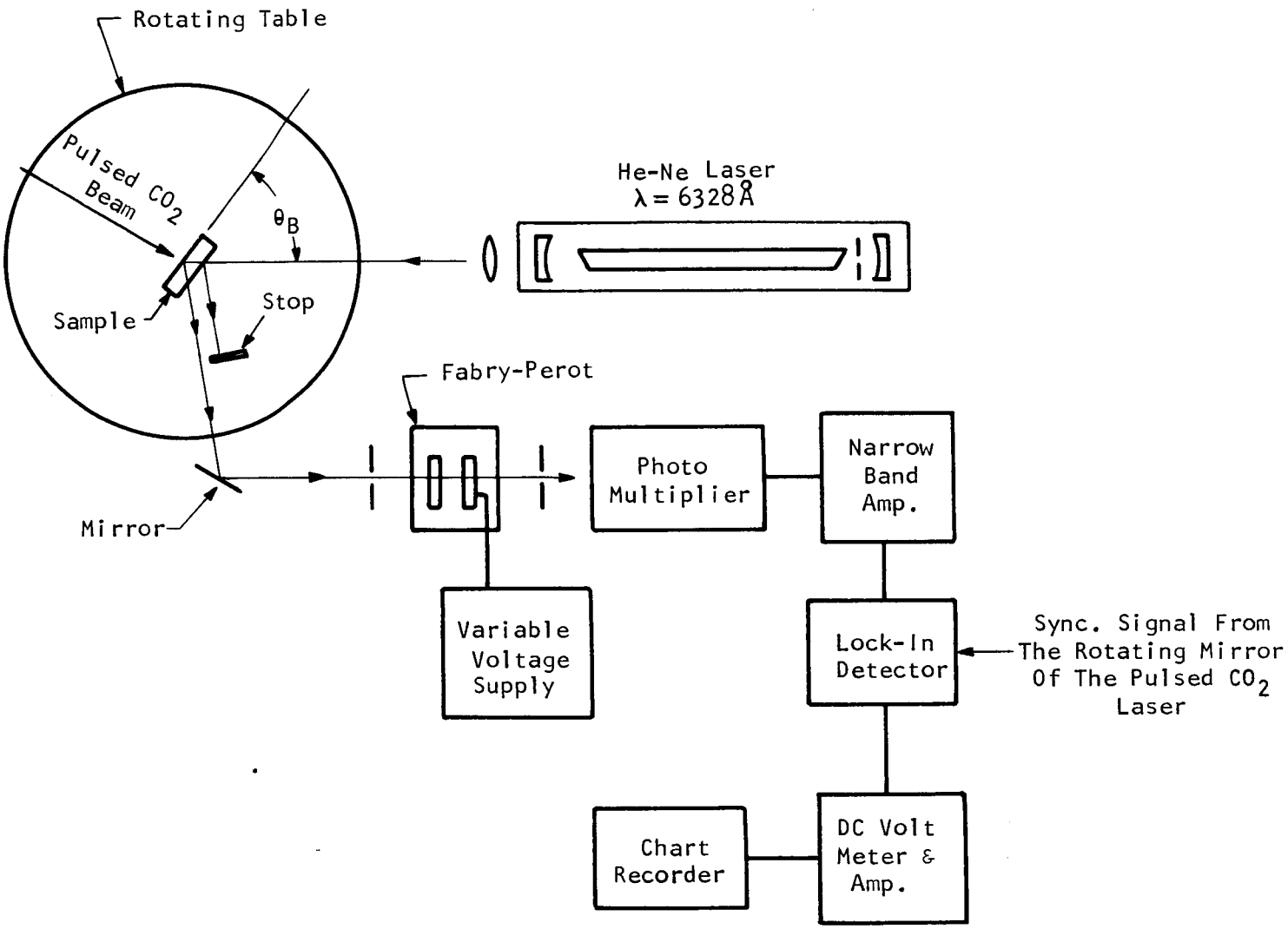

Fig. 9—Experimental arrangement in the search for 54 GHz acoustic waves in saphire

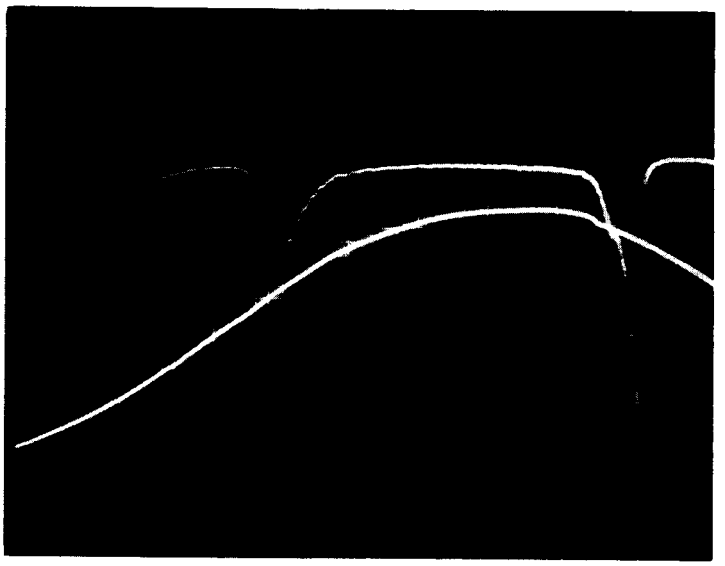

Fig. 10—Fabry-Perot scan of the He-Ne laser light operating at $\lambda = 6328$ Å. The Fabry-Perot spacing was 1.55 cm

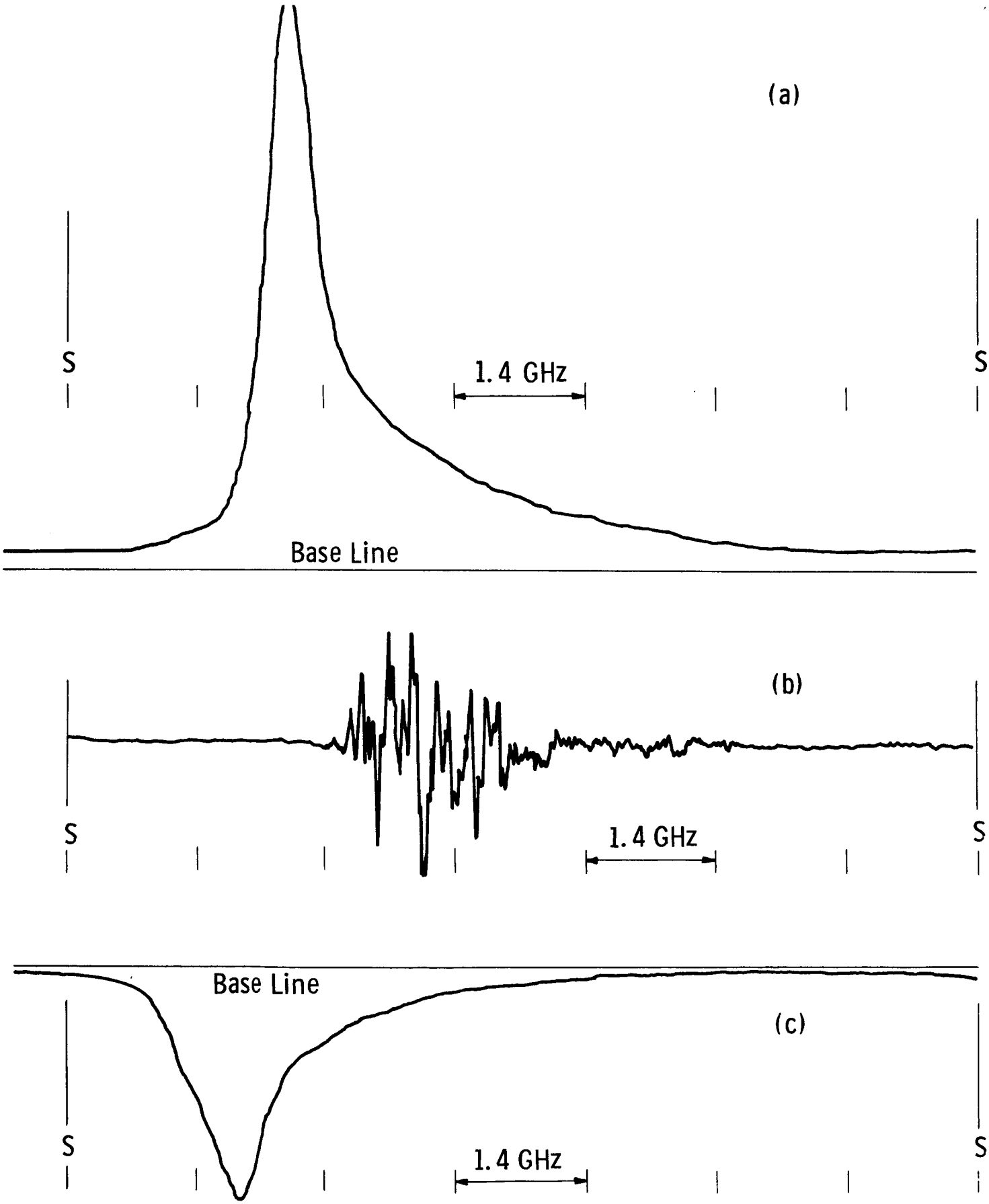

Fig. 11—(a) Fabry-Perot Scan of He-Ne Laser Light
(b) Fabry-Perot Scan of 400 Hz Noise Inherent in the He-Ne Laser Light
(c) Fabry-Perot Scan of 400 Hz Signal Caused by the CO_2 Laser Beam

where the vertical lines marked "S" engulf one special range. For Fig. 11a, the output of the photomultiplier is fed directly into a DC μ-ammeter. The peak of the signal corresponds to the center frequency of the laser light, and it can be seen that at a frequency 5.8 GHz away from the laser frequencies the background light is reduced significantly. Figure 11b shows the 400 Hz noise inherent in the laser light and Fig. 11c shows the 400 Hz signal obtained when the CO_2 laser is allowed to hit the sapphire sample. As can be seen, there is a net 400 Hz signal in the He-Ne laser light which is reflected from the back surface of the sample. And, it was determined that this net signal was not frequency shifted by the acoustic frequency. Since sapphire absorbs the CO_2 light strongly, this amplitude modulation of the reflected laser light is probably caused by heating effects at the surface which distort the surface at the 400 Hz repetition rate. This serious problem which exists for sapphire would not exist for samples which are transparent to the CO_2 laser light (10.6μ).

That the heating effect and laser noise destroy all hope of seeing the Bragg effect can be shown by the following calculations. It will be assumed that the CO_2 spot size has an area of 10^{-5} cm^2, that is, h^2 will be taken as 10^{-5} in Eq. (6). K_i will be taken as 1.765×10^5 cm^{-1} and a value of $p_{21} \sim 0.3$ will be assumed. A strain of 10^{-6} will also be assumed. θ_B for a-cut sapphire and 54 GHz longitudinal waves is ~61°. For the above values and the use of Eqs. (6) and (7) it is found that

$$\frac{I_D}{I_0} \sim 5 \times 10^{-8}$$

during the pulse of acoustic energy. The heating effect induces a signal 10^4 times larger than the calculated Bragg effect. Therefore, even if this signal were noiseless it would have to be bucked out. It is also known from past experience that laser amplitude noise in a narrow band of frequencies (1 sec time constant) at the 400 Hz rate is of the order 10^{-4} to 10^{-5} compared to the laser intensity I_0. Because of the cw reflected light from the back surface, this noise is always present. Therefore, a large improvement in signal-to-noise could be realized in the above experiment if the He-Ne laser were to be turned on only during the time that the CO_2 laser is on. Needless to say, the Bragg light was not seen after a fairly complete search within a small angular range centered about the theoretical Bragg angle.

Future Plans

$\Omega \lesssim \Omega_B$ -- For acoustic frequencies less than but near Ω_B, because of the high acoustic attenuation, it was shown that specular reflection from the acoustic excitation surface seriously complicates the observation of the Bragg light. In the first attempt a Fabry-Perot interferrometer was used to try to separate the frequency shifted and unshifted beams. In the future many changes can be made. First the sample will be cooled. For sapphire cooling from room temperature down to $T < 30^{\circ}K$ results in a reduction of α by at least a factor of 10. Samples that exhibit low absorption of CO_2 laser light will be considered in order to prevent serious heating effects. It is also possible to

separate the Bragg light from the laser beam by using polarization isolation.[22] That is, the Bragg light under certain conditions can have a different polarization than the incident laser beam. Lastly, for acoustic frequencies greater than 10 GHz, it will be feasible to use high resolution monochromators to separate two light beams differing by the acoustic frequency. It should also be pointed out that as Ω is increased, the wavelengths of the detecting light can be, in principle, decreased such that the condition $\Omega < \Omega_B$ is always satisfied. Because of existing equipment only red light (λ_L = 6328 Å) has been considered so far. Argon lasers (λ_L = 4880 Å) and x-rays will also be considered for future experiments. It can be seen from Eq. (6) that the Bragg diffracted intensity varies as λ_L^{-2}; therefore, there is a gain in diffracted power, for any given acoustic frequency, as λ_L is decreased. Work towards most of these changes is currently in progress.

$\Omega > \Omega_B$ -- For this frequency range the idea of Bragg scattering has to be given up completely. There are, however, two possible ways to observe sound waves in samples for $\Omega > \Omega_B$. The first method involves surface reflection. Instead of coherent multiple scattering from many wavefronts, as is the case with Bragg scattering, only one surface is used to scatter the laser light. This one surface can in fact be the acoustic excitation surface. Since this surface is moving at the acoustic frequency, the surface will Doppler shift a small portion of the reflected light. All of the methods of separating 2 beams of light differing by the acoustic frequency mentioned above can be used to see the shifted

light although the effect would be at least 100 times harder to see than Bragg scattering.

The second method involves a volume of $\lambda_s/2$ in depth in back of the excitation surface. This layer of material is polarized by the detecting light and re-radiates light which is shifted in frequency due to the acoustic wave. This radiation is emitted in all 4π steradians and can be observed in directions which do not contain the specularly reflected laser beam from the surface. Unshifted background light due to the Raleigh scattering again makes it important to have some way to separate light according to its frequency. Rough calculations indicate that the frequency shifted component radiated in all 4π steradians is 10^{-7} compared to I_0 for strains of 10^{-6}.

References

1. J.M. Ziman, Electrons and Phonons (Oxford Press, 1960).
Thor A. Bak, Ed., Phonons and Phonon Interactions, Aarhus Summer School Lectures, 1963 (W.A. Benjamin, Inc., 1964).
2. B. Carlin, "The Use of High- and Low-Amplitude Ultrasonic Wave for Inspection and Processing," Physical Acoustics, Vol. 1, Part A, W.P. Mason, Ed. (Academic Press, 1965), Chap. I.
C.F. Brockelsby, J.S. Palfreeman and R.W. Gibson, Ultrasonic Delay Lines (London Iliffe Books Ltd., 1963).
3. For a detailed discussion of these relationships and their tensor character see; J.F. Nye, Physical Properties of Crystals (Oxford Press, 1957) and L.D. Landau and E.F. Lifshitz, Electrodynamics of Continuous Media (Pergamon Press, 1960).
4. H.J. McSkimn, "Ultrasonic Methods for Measuring the Mechanical Properties of Liquids and Solids," Physical Acoustics, Vol. 1, Part A, W.P. Mason, Ed. (Academic Press, 1965), Chap. 4.
5. J. de Klerk, "Fabrication of Vapor-Deposited Thin Film Piezoelectric Transducers for the Study of Phonon Behavior in Dielectric Materials at Microwave Frequencies," Physical Acoustics, Vol. IV, Part A, W.P. Mason, Ed. (Academic Press, 1966), Chap. 5.
6. L. Bergman, Ultrasonics (John Wiley & Sons, Inc., 1940), Chap. II.
A. Barone, "Generation, Detection and Measurement of Ultrasound," Handbuch Der Physik, S. Flugge, Ed., Vol. XI, Acoustics II (Springer-Verlag, 1962), Chap. II.

7. W.G. Mayer and E.A. Hiedemann, J. Acous. Soc. Am. 30, 757 (1958).
J.H. Parker, Jr., E.F. Kelly and D.I. Bolef, Appl. Phys. Letts. 5, 7 (1964).

8. K.N. Baranski, Soviet Physics - Doklady 2, 237 (1958).

9. R. Loudon, "The Raman Effect in Crystals," Advances in Physics 13, 423 (1964).

10. R.Y. Chiao, C.H. Townes and B.P. Stoicheff, Phys. Rev. Letts. 12, 592 (1964).

11. D.E. Caddes, C.F. Quate and C.D.W. Wilkinson, Appl. Phys. Letts. 8, 309 (1966).

12. C.K.N. Patel, Phys. Rev. 136, A1187 (1964).

13. G. Birnbaum, Optical Masers, (Academic Press, 1964).
W.V. Smith and P.P. Sorokin, The Laser (McGraw-Hill Book Co., 1966).

14. C.K.N. Patel, Phys. Rev. 136, A1187 (1964).
J.D. Rigden and G. Moeller, J. Quant. Elect. QE2, 365 (1966).
W.J. Witteman, J. Quant. Elect. QE2, 375 (1966).
G.W. Flynn, L.O. Hocker, A. Javan, M.A. Kovacs and C.K. Rhodes, J. Quant. Elect. QE2, 378 (1966).
C.K.N. Patel, P.K. Tien and J.H. McFee, Appl. Phys. Letts 7, 290 (1965).

15. M.A. Kovacs, G.W. Flynn and A. Javan, Appl. Phys. Letts 8, 62 (1966).
C.K.N. Patel, Phys. Rev. Letts. 16, 613 (1966).

16. C.F. Quate, C.D.W. Wilkinson and D.K. Winslow, Proc. IEEE 53, 1604 (1965).

17. John C. Slater, Rev. Mod. Phys. 30, 197 (1958).

18. J. de Klerk, Phys. Rev. 139, A1635 (1965).

19. R.L. Fork, D.R. Herriott and H. Kogelnik, Applied Optics 3, 1471 (1964).

20. J. de Klerk and E.F. Kelly, R.S.I. 36, 506 (1965).

21. Sumner P. Davis, Applied Optics 2, 727 (1963).

22. R.W. Dixon, J. Quant. Elect. QE3, 85 (1967).

APPENDIX I

Decay of High Frequency Longitudinal Phonons

by

P. G. Klemens

DECAY OF HIGH-FREQUENCY LONGITUDINAL PHONONS*

P. G. Klemens

Abstract

The anharmonic decay of a high-frequency longitudinal elastic wave at low temperatures, such that $\hbar\omega > KT$, is calculated by perturbation theory, using a Grueneisen parameter as measure of the anharmonicity. The attenuation at very low temperatures varies as the fifth power of frequency, and is small at frequencies below 10^{12} Hz.

*This work was supported by the National Aeronautics & Space Administration, under Contract No. NAS8-18023.

ANHARMONIC INTERACTIONS

We consider a wave of frequency ω interacting with other modes owing to the cubic anharmonicities. The perturbation Hamiltonian due to cubic anharmonicities can be expressed in the form[3]

$$H' = c_3 \, a(\underline{q}) \, a^*(\underline{q}') \, a^*(\underline{q}'') \tag{1}$$

where $a(\underline{q})$, $a^*(\underline{q})$ are the phonon annihilation and creation operators, c_3 is a coefficient to be discussed below, and the displacement of a point $\underline{x}$ due to a lattice wave of wave-vector $\underline{q}$ and frequency ω is expressed as

$$\underline{u}(\underline{x}) = \frac{1}{\sqrt{G}} \, \underline{\epsilon} \, e^{i\underline{q}\cdot\underline{x}} \, a(\underline{q}) \tag{2}$$

where G is the number of atoms in the crystal, and $\underline{\epsilon}$ is a unit vector defining the polarization direction. One can then show that the energy of each mode consists of N phonons, so that

$$E_{\underline{q}} = \frac{1}{2} M\omega^2 \left[a^*(\underline{q}) \, a(\underline{q}) + a(\underline{q}) \, a^*(\underline{q}) \right]$$

$$= \hbar\omega \left(N_{\underline{q}} + \frac{1}{2} \right) \tag{3}$$

and one can further show that the rate of change of N, the number of phonons in mode $\underline{q}$, is given by

$$t \frac{dN}{dt} \Big] = \sum_{\underline{q}', \underline{q}''} 2 |c_3|^2 \frac{\hbar^3}{M^3 \omega\omega'\omega''} \frac{1 - \cos \Delta\omega t}{\hbar^2 \Delta\omega^2} \Big[(N+1)N'N'' - N(N'+1)(N''+1)\Big] \tag{4}$$

where M is the atomic mass and

$$\Delta\omega = \omega - \omega' - \omega'' \tag{5}$$

If the anharmonicity is the same in all regions of the crystal, and if we confine ourselves to waves long compared to the interatomic distance, so that Umklapp processes play no role, the coefficient c_3 vanishes unless the following interference condition is satisfied

$$\underline{q} = \underline{q}' + \underline{q}'' \tag{6}$$

The magnitude of c_3 depends on the nature of the anharmonic forces. On the basis of a simplified Grueneisen model one obtains the following approximate expression[3]

$$c_3 = 2\gamma(3G)^{-1/2} \, Mv^2 \, q \, q' \, q'' \tag{7}$$

where v is the sound velocity. One thus obtains in place of (4)

$$t \frac{dN}{dt} \Big] = \sum_{\underline{q}'} \frac{8\gamma^2}{3G} \frac{\hbar}{Mv^2} \omega\omega'\omega'' \frac{1 - \cos \Delta\omega t}{\Delta\omega^2} \Big[(N+1)N'N'' - N(N'+1)(N''+1)\Big] \tag{8}$$

The summation extends over all modes $\underline{q}'$ (including different polarizations) and over all polarizations of $\underline{q}''$, but the wave-vector $\underline{q}''$ is determined by (6). Equation (8) formally accounts only for processes in which a phonon $\underline{q}$ splits into $\underline{q}'$ and $\underline{q}''$, i.e. $\underline{q} \longleftrightarrow \underline{q}' + \underline{q}''$, but one can also take account of processes $\underline{q} + \underline{q}' \longleftrightarrow \underline{q}''$ by changing the sign of ω' and $\underline{q}'$ in (5) and (6) respectively, and by changing N' to $(N'+1)$ and $(N'+1)$ to N' in equation (8).

DECAY OF LONGITUDINAL PHONON

Let us suppose now that mode $\underline{q}$ is a longitudinal wave, that $\hbar\omega > KT$, and that the medium is an isotropic elastic continuum, so that $\omega'/q' = v$, the sound velocity. We distinguish between v_I and v_{II}, the velocity of longitudinal and transverse waves.

The resonance factor $(1 - \cos \Delta\omega t)/\Delta\omega^2$ in (8) ensures that only these processes contribute to $dN/dt]$ for which $\Delta\omega$ of eq. (5) vanishes. The requirement $\Delta\omega = 0$, together with the selection rule (6), allows only processes of the following type to occur

$$L \longleftrightarrow T + T \qquad (9a)$$

$$L \longleftrightarrow L + T \qquad (9b)$$

$$L \longleftrightarrow L - T \qquad (9c)$$

where L denotes a longitudinal phonon, T a transverse phonon. There is a double degeneracy associated with each transverse phonon; there are thus 4 interactions of type (9a), two of type (9b) and two of type (9c).

Interaction (9b) and (9c) is really the same interaction, but in (9b) the longitudinal mode $\underline{q}$ can occur in two places; if we require $\underline{q}$ to be on the left-hand side of equations (9), we must distinguish between processes (9b) and (9c). Processes of type (9a) and (9b) correspond to phonon $\underline{q}$ splitting into two phonons; these processes can occur even at the absolute zero of temperature. Processes (9c) require the prior presence of a transverse phonon; therefore they occur only at finite temperatures, not at absolute zero.

Consider first processes of type (9a). The locus of points $\underline{q}'$ such that $\Delta\omega = 0$ is an ellipsoid of revolution, for $\omega' = v_{II}q'$, $\omega'' = v_{II}q''$, $\omega = v_I q$, the wave-vectors are related by (6) and their magnitudes by

$$q' + q'' = \frac{v_I}{v_{II}}\, q \tag{10}$$

The ellipsoid is generated by rotating the ellipse of Fig. 1 about OQ; O and Q are the foci and the distance of OQ is q.

The summation in (8) can now be written

$$\sum_{\underline{q}'} = \frac{4Ga^3}{(2\pi)^3} \int d^3\underline{q}' \tag{11}$$

where a^3 is the atomic volume, so that Ga^3 is the volume of the crystal, while the factor 4 arises from the sum over the polarizations of $\underline{q}'$ and $\underline{q}''$. Now $\Delta\omega = 2v_{II}\,\delta q_n$ at points A and B and $\sqrt{2}\, v_{II}\,\delta q_n$ at C, where

δq_n is an increment of $\underline{q}'$ normal to the surface $\Delta\omega = 0$. At intermediate points the expression for $\Delta\omega$ is more complicated. If we, rather arbitrarily, replace the ellipse by a sphere of radius $q/2$, and regard the value of $\Delta\omega$ at C to be typical for the whole surface, then we obtain an approximate value of

$$\int d^3\underline{q}' = 4\pi \left(\frac{q}{2}\right)^2 dq_n$$

$$= 4\pi \left(\frac{q}{2}\right)^2 \frac{1}{\sqrt{2}\, v_{II}} \, d(\Delta\omega) \qquad (12)$$

This can now be substituted into (8), and the following relation can be used

$$\int \frac{1 - \cos \Delta\omega t}{\Delta\omega^2} \, d(\Delta\omega) = \pi t \qquad (13)$$

To deal with the factor in square brackets in (8) we assume that N' and N" are at their equilibrium values. In the case of an ultrasonic wave N is much larger than its equilibrium value, and only the term linear in N need be considered. Thus

$$(N+1)N'N'' - N(N'+1)(N''+1) = -N(N'+N''+1) \qquad (14)$$

The decay rate $1/\tau$ of the ultrasonic wave is defined by

$$\frac{1}{\tau} = -\frac{1}{N} \frac{dN}{dt} \Bigg] \qquad (15)$$

In the integration over the surface of the ellipsoid, q' and q" take up different values separately, even though q' + q" is constant. As a further simplification we assume the values of q' and q" to be constant and appropriate to the value at point C, i.e. $\omega' = \omega'' = \omega/2$, or $q' = q'' = (v_I/v_{II})\, q/2$. With this simplification we combine (8), (11), (12), (13) and (14) and obtain after some reduction

$$\frac{1}{\tau} = \gamma^2 \frac{\hbar\omega}{Mv^2}\,\omega\,\frac{1}{12\pi\sqrt{2}}\,\frac{v_I}{v_{II}}\,q^3 a^3\,(N'+N''+1)$$

$$= \gamma^2 \frac{\pi}{2\sqrt{2}}\,\omega\,\frac{\hbar\omega}{Mv^2}\left(\frac{\omega}{\omega_D}\right)^3 \frac{v_I}{v_{II}}\,(N'+N''+1) \qquad (16)$$

where ω_D is the longitudinal Debye frequency, defined by $\omega_D = v_I q_D$ and $a^3 q_D^3 = 6\pi^2$.

At the absolute zero of temperature $(N'+N''+1) = 1$. More generally, if it is again assumed for simplicity that $\omega' = \omega'' = \omega/2$

$$(N'+N''+1) = 1 + 2/[e^{\hbar\omega/2KT} - 1]$$

$$\simeq 1 + 4KT/\hbar\omega \qquad \text{if} \quad KT > \tfrac{1}{2}\hbar\omega \qquad (17)$$

We must now consider the effect of processes (9b) and (9c). To be definite let $\underline{q}$ be the L-mode on the left-hand side of (9), let $\underline{q}'$ be the T-mode (two cases) and let $\underline{q}''$ be the L-mode on the right-hand side of (9b) or (9c).

The locus of $\underline{q}'$ is the surface of revolution generated by rotating the curve of Fig. 2 about the axis OQBC. This curve consists of two branches. The smaller branch, passing through B, corresponds to processes (9b); the larger branch, passing through C, corresponds to (9c).

The position of B or the magnitude of q' is given by

$$v_I q = v_{II} q' + v_I (q'-q) \tag{18}$$

since $q'' = q' - q$. Thus $q' = 2q/(1 + \alpha)$, where $\alpha = v_{II}/v_I$. Typically $\alpha = 2/3$ and $q' = 1.2q$. Similarly the position of C is given by

$$v_I q + v_{II} q' = v_I (q'-q) \tag{19}$$

or $q' = 2q/(1 - \alpha)$. Typically q' is then about 6q.

If $\underline{q}'$ is perpendicular to $\underline{q}'$, one readily finds that $(q'/q) = 0$ or $2\alpha/(1 - \alpha^2)$; this determines the position of D. If $\underline{q}''$ is perpendicular to $\underline{q}$, one finds that

$$\frac{q''}{q} = \frac{1 \pm \sqrt{1 - (1 - \alpha^2)^2}}{1 - \alpha^2} \tag{20}$$

this determines the position of E and E' respectively. Thus if $\alpha = 2/3$, $q''/q \simeq 3.3$ in case (9c).

These quantities determine the approximate dimensions of the locus of $\underline{q}'$ as drawn in Fig. 2.

The surface of the branch OB is comparable to the surface of Fig. 1. Since there are only two possible polarization combinations,

the contribution of that branch (processes 9b) to the attenuation rate is about half the contribution from processes (9a); furthermore, this contribution will have a similar temperature dependence.

The contribution from processes (9c) is much more difficult to estimate. However, since these processes require the prior presence of transverse phonons, they can be disregarded at the absolute zero of temperature. At elevated temperatures, however, they will dominate the interaction process. Since the surface area of that branch exceeds that of Fig. 1 by a factor of order 10, we may write the total attenuation in the form

$$\frac{1}{\tau} = \frac{3\pi}{4\sqrt{2}} \gamma^2 \omega \frac{\hbar\omega}{Mv^2} \left(\frac{\omega}{\omega_D}\right)^3 \frac{v_I}{v_{II}} \left[1 + \frac{4KT}{\hbar\omega} + F(T)\right] \qquad (21)$$

Here we have increased the result of (16) by a factor 3/2 to include processes (9b) as well as (9a), and approximated the temperature dependence (17) by the high-frequency limit. The additional term F(T) describes processes (9c). We have no accurate knowledge of F(T), but expect it to show the following qualitative characteristics:

At $T = 0$, $F(T) = 0$. When $KT < \hbar\omega$, F(T) should vary as some power of T; since the major contributions would then come from the region near 0, when the locus of $\underline{q}'$ is cone-shaped, the behavior should be similar to the attenuation of a transverse wave,[4,5] so that

$$F(T) \simeq \left(\frac{KT}{\hbar\omega}\right)^4 \qquad (22)$$

In this region F(T) is still a relatively small correction. The increase of F(T) with T should be considerably slower than given by (22) once KT is comparable to $\hbar\omega$. At higher temperatures F(T)/T should saturate, reflecting the closed form of the branch ODC; since this branch has an area typically 30 times that of the branch OE'B, and since the latter branch contributes about 1/3 of the second term in (21), we would expect

$$F(T) \simeq \frac{40\ KT}{\hbar\omega} \tag{23}$$

as $KT > \hbar\omega$.

SOME NUMERICAL CASES

Let us consider a typical solid of $\gamma = 2$, $Mv^2/K \simeq 50{,}000^\circ K$, $v_I/v_{II} = 3/2$, and a Debye temperature $\theta \simeq 1000^\circ K$. At the absolute zero of temperature the anharmonic decay rate then becomes

$$\frac{1}{\tau} = 10\omega \left(\frac{\nu}{20}\right)^4 \frac{1}{5 \times 10^4 \times (10^3)^3} \text{ sec}^{-1}$$

$$= 10^{-18}\ \nu^4\omega \text{ sec}^{-1} \tag{24}$$

where ν is the frequency expressed in GHz (noting that 20 GHz corresponds to $1^\circ K$), while ω is the frequency in radians/sec. The attenuation coefficient α is $(v_I\tau)^{-1}$, and taking $v_I \simeq 10^6$ cm/sec,

$$\alpha = 10^{-24}\ \nu^4\omega \quad \text{cm}^{-1}$$

$$= 6 \times 10^{-15}\ \nu^5 \quad \text{cm}^{-1} \tag{25}$$

Thus the anharmonic attenuation length $1/\alpha$ is many centimeters even at frequencies as high as 100 GHz. In practice, the attenuation of such waves in samples of ordinary dimensions is probably governed by surface irregularities. It is only when the 1000 GHz region is reached that the anharmonic processes discussed here would form an important attenuation mechanism at low temperatures (in that case well below $50^{\circ}K$).

At higher temperatures the anharmonic processes will be more important. In quartz ($\theta = 600^{\circ}K$, $Mv^2/K = 50{,}000^{\circ}K$, $v_I = 6 \times 10^5$ cm/sec) and at 114 GHz one would expect α to be about 1×10^{-3} cm^{-1} at $T = 0$ and about 1×10^{-1} at $10^{\circ}K$. Ilukor and Jacobson[2] found an anharmonic attenuation about a factor 10 larger at that temperature and frequency. The discrepancy may well be due to collinear processes of the type $L \leftrightarrow L + L$, which we have not considered here, but which play a large role at lower frequencies.[6,7] These processes can be important when $KT > \hbar\omega$, though they should lead to an attenuation proportional to the first power of frequency, and the extra attenuation found by Ilukor and Jacobson is considerably higher than would be indicated by an extrapolation from the results of Thaxter and Tannenwald[1] at 70 GHz.

Clearly one needs not only a better theory, particularly calculations for the awkward region $\hbar\omega \simeq KT$, but also more experimental data.

REFERENCES

1. J.B. Thaxter and P.E. Tannenwald, Appl. Phys. Letters 5, 67 (1964).
2. J. Ilukor and E.H. Jacobson, Science 153, 1113 (1966).
3. P.G. Klemens, Solid State Physics 7, 1 (1958).
4. L. Landau and G. Rumer, Physik. Z. Sowjetunion 11, 18 (1937).
5. P.G. Klemens in "Physical Acoustics," vol. III b, p. 201, Academic Press, New York, 1965.
6. H.J. Maris, Phil. Mag. 9, 901 (1964).
7. P.G. Klemens, to be published.

FIGURE CAPTIONS

Fig. 1 Locus of $\underline{q}'$ for processes (9a): $\underline{q} = \underline{q}' + \underline{q}''$, $\underline{q}$ is longitudinal, $\underline{q}'$ and $\underline{q}''$ are transverse.

Fig. 2 Locus of $\underline{q}'$ for processes (9b) and (9c): $\underline{q} = \underline{q}' + \underline{q}''$ for branch OE'B, $\underline{q} + \underline{q}' = \underline{q}''$ for branch ODEC; $\underline{q}$ and $\underline{q}''$ are longitudinal, $\underline{q}'$ is transverse, the length OQ is equal to q.

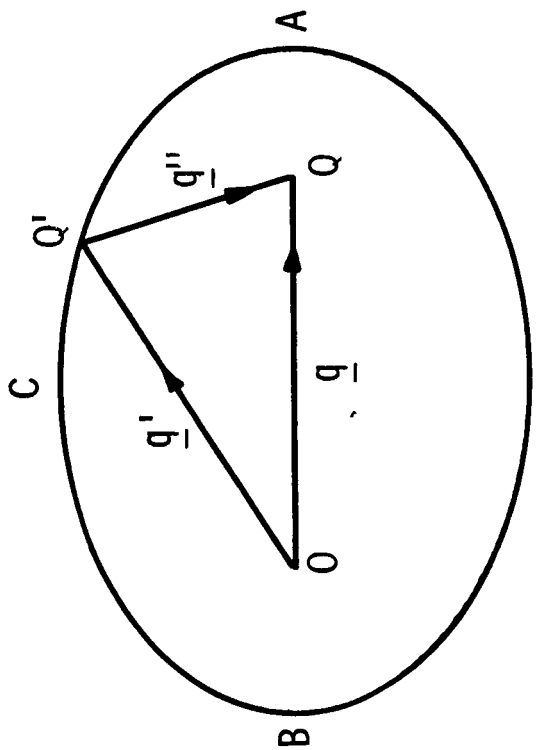

Fig. 1

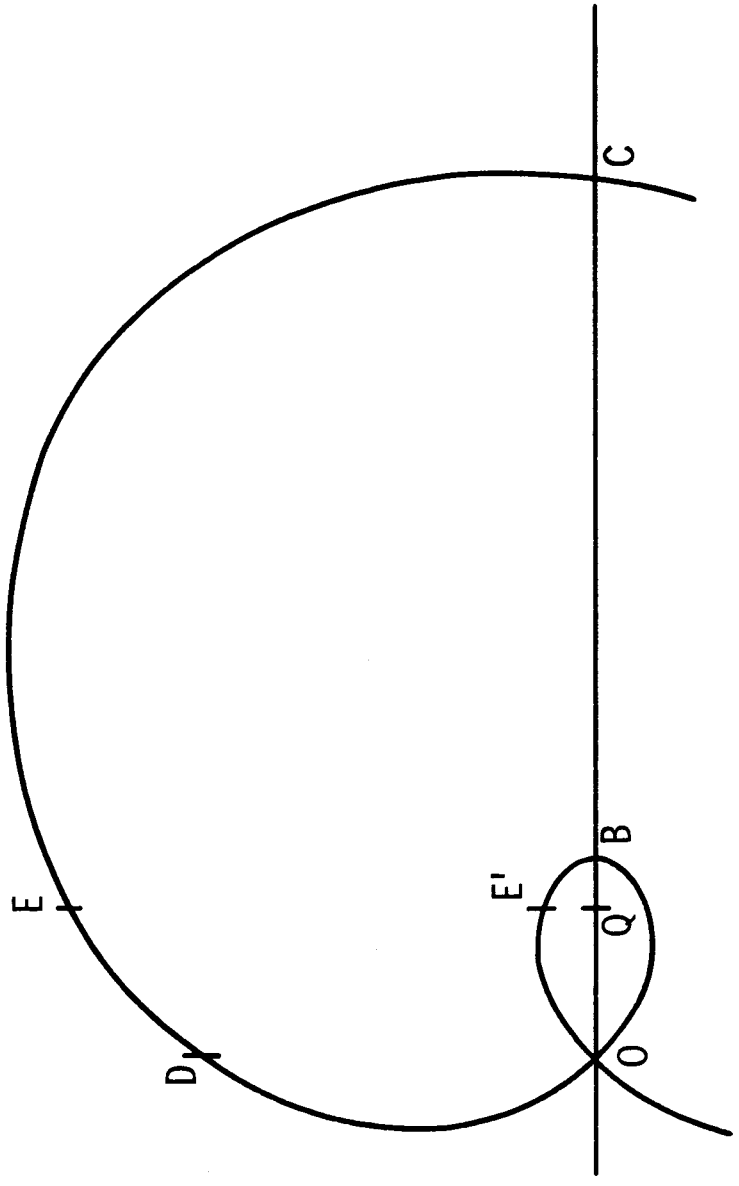

Fig. 2